ORGANOMETALLICS

Article

pubs.acs.org/Organometallics

Diacetylplatinum(II) Complexes with κ^2-Coordinated Tris(pyridyl)methanol and Tris(pyridyl)methyl Ether Ligands: Structural Insight into the Ligand Dynamics in Solution

Martin Bette,[†] Tim Kluge,[†] Jürgen Schmidt,[‡] and Dirk Steinborn*[,†]

[†]Institute of Chemistry-Inorganic Chemistry, Martin Luther University of Halle-Wittenberg, Kurt-Mothes-Straße 2, D-06120 Halle, Germany

[‡]Department of Bioorganic Chemistry, Leibniz Institute of Plant Biochemistry, Weinberg 3, D-06120 Halle, Germany

Supporting Information

ABSTRACT: Reactions of the bis(benzylamine)platinum(II) complex $[Pt(COMe)_2(NH_2Bn)_2]$ (**2**; Bn = benzyl) with (2-py)$_3$COR (2-py = 2-pyridyl), (2-py)$_2$PhCOR, and (2-py)$_2$(*m*-Tol)COR (*m*-Tol = 3-methylphenyl) afforded the neutral diacetylplatinum(II) complexes $[Pt(COMe)_2\{(2\text{-py})_3COR\}]$ (R = H (**3a**), Me (**3b**), Et (**3c**), Bn (**3d**)), $[Pt(COMe)_2\{(2\text{-py})_2PhCOR\}]$ (R = H (**4a**), Me (**4b**)), and $[Pt(COMe)_2\{(2\text{-py})_2(m\text{-Tol})COR\}]$ (R = H (**5a**) Me (**5b**)), respectively, having, due to a κ^2 coordination of the ligands, a 2-pyridyl (**3**), a phenyl (**4**), or a *m*-tolyl (**5**) ring as the pendant group. The identities of all complexes were unambiguously proved by high-resolution mass spectrometric investigations and by NMR (^{1}H, ^{13}C, ^{195}Pt) and IR spectroscopy as well as by single-crystal X-ray diffraction analyses (**3a**−**d**). In methanol solution, complexes **3b**−**d** and **5b** show a dynamic behavior. The thermodynamic parameters of these dynamics have been determined by variable-temperature ^{1}H NMR measurements (Eyring plots). Furthermore, extensive DFT calculations will be presented, which indicate that the dynamics are caused by the interplay of hindered and respectively unhindered rotations of the substituent R and/or the pendant group.

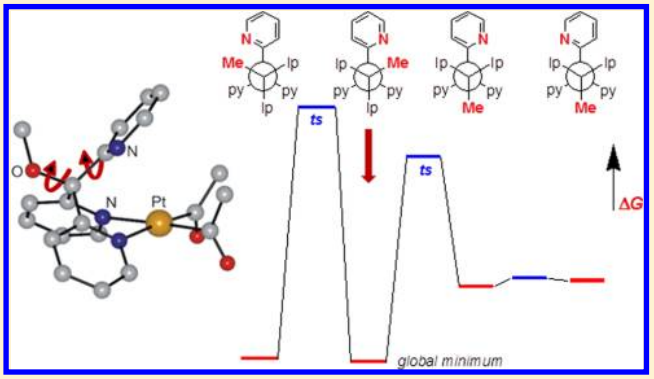

1. INTRODUCTION

The dinuclear platina-β-diketone $[Pt_2\{(COMe)_2H\}_2(\mu\text{-}Cl)_2]$ (**1**), being accessible by the reaction of hexachloridoplatinic acid with *n*-butyl alcohol and bis(trimethylsilyl)acetylene, can be considered as a hydroxycarbene complex, where the hydroxycarbene ligands are stabilized by intramolecular O−H···O hydrogen bonds to neighboring acetyl ligands (Scheme 1, **a**).[1] Due to its electronic unsaturation (16 valence electrons) and kinetically labile ligand sphere, the platina-β-diketone **1** exhibits a unique reactivity and thus is a suitable precursor complex for the synthesis of a great variety of acetyl platinum(II) and platinum(IV) complexes with bidentate N^N, P^P, S^S, and N^O ligands.[2] Thus, the reaction of complex **1** with the bidentate *N*-donor 2,2′-bipyridine leads to the formation of the thermally extraordinarily stable diacetyl(hydrido)platinum(IV) complex **I** (Scheme 1, **b**), which affords with NaOH a reductive elimination of HCl to form the respective diacetylplatinum(II) complex **II** (Scheme 1, **c**).[3] Reactions of **1** with tris(pyrazolyl)borates (so-called scorpionates)[4] and tris(pyrazolyl)methanes, which represent examples of tridentate *N*-donor ligands, followed by the addition of a base led in an analogous manner to the formation of the diacetylplatinum(II) complexes **III** and **IV** bearing the tripodal ligand only κ^2N,N' coordinated with a pendant pyrazolyl ring (Scheme 1, **d** and **e**).[5,6] Due to its substitution-labile benzylamine ligands, the bis(benzylamine)platinum(II) complex **2**, accessible by the reaction of **II** in neat benzylamine (Scheme 1, **f**), was found to be another useful precursor complex for the synthesis of diacetylplatinum(II) complexes.[7] In this reaction pathway diacetylplatinum(II) complexes **III** bearing scorpionate ligands could also be synthesized but, unexpectedly, not the type **IV** complexes (Scheme 1, **g** and **h**).[5,6]

Both types of ligands, the anionic tris(pyrazolyl)borates as well as the isoelectronic neutral tris(pyrazoyl)methanes, are—due to the tetrahedral geometry at their central B or C backbone atom—restricted to a facial κ^3N,N',N'' coordination in octahedral complexes. For the same reason the coordination mode of these ligands in type **III** and **IV** square-planar complexes is κ^2N,N' with a pendant third pyrazolyl ring.[4,8] Although these ligands are isoelectronically and structurally very similar, their diacetylplatinum(II) and -platinum(IV) complexes may exhibit great differences in reactivity and chemical behavior.[5,6]

Received: February 1, 2013

   dx.doi.org/10.1021/om400091h | *Organometallics* XXXX, XXX, XXX−XXX

Scheme 1. Synthesis of Diacetylplatinum(II) Complexes Bearing κ^2-Bonded Scorpionate (III) and Tris(pyrazolyl)methane Ligands (IV)

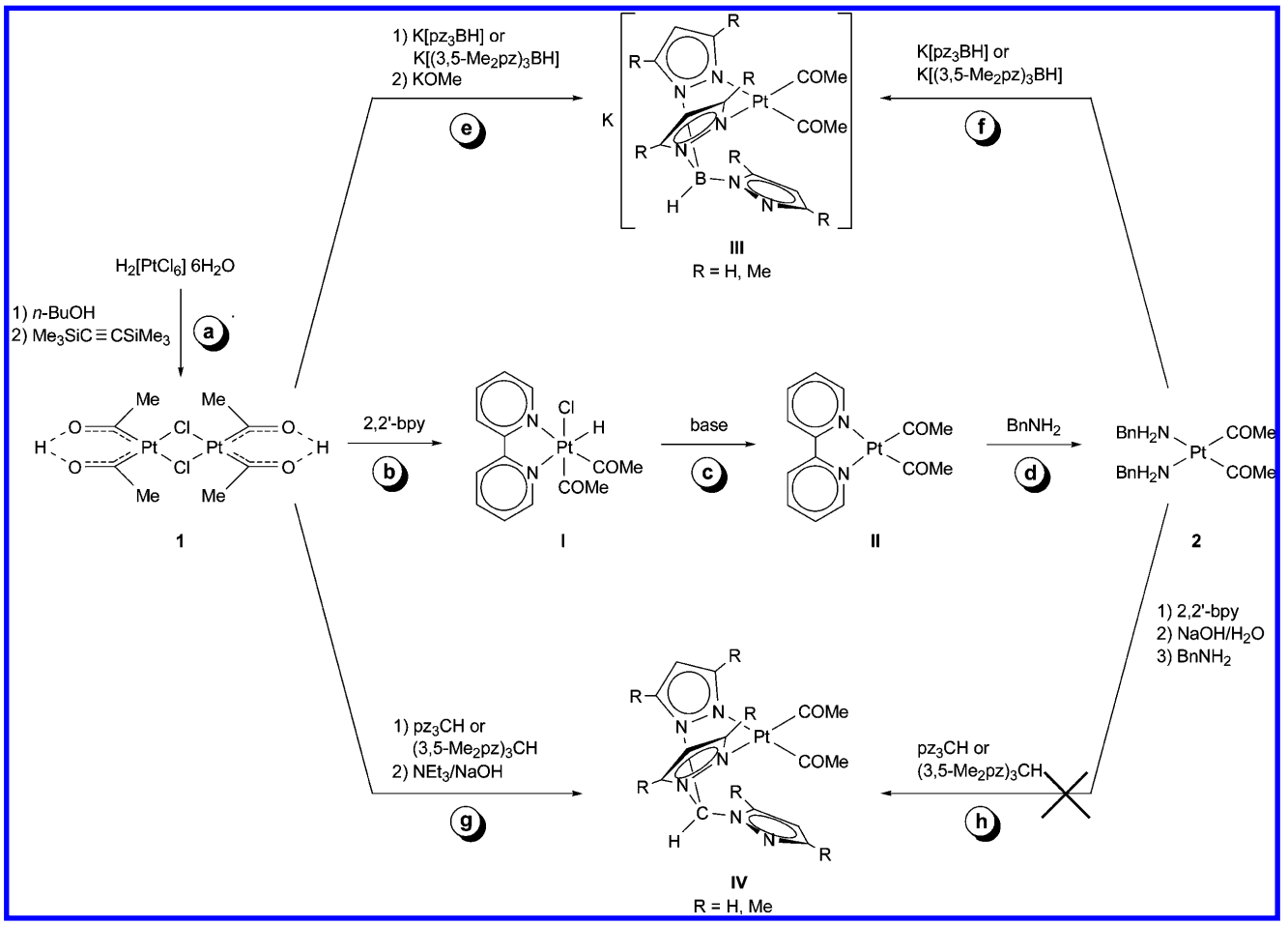

Scheme 2. Syntheses of the Diacetylplatinum(II) Complexes 3–5

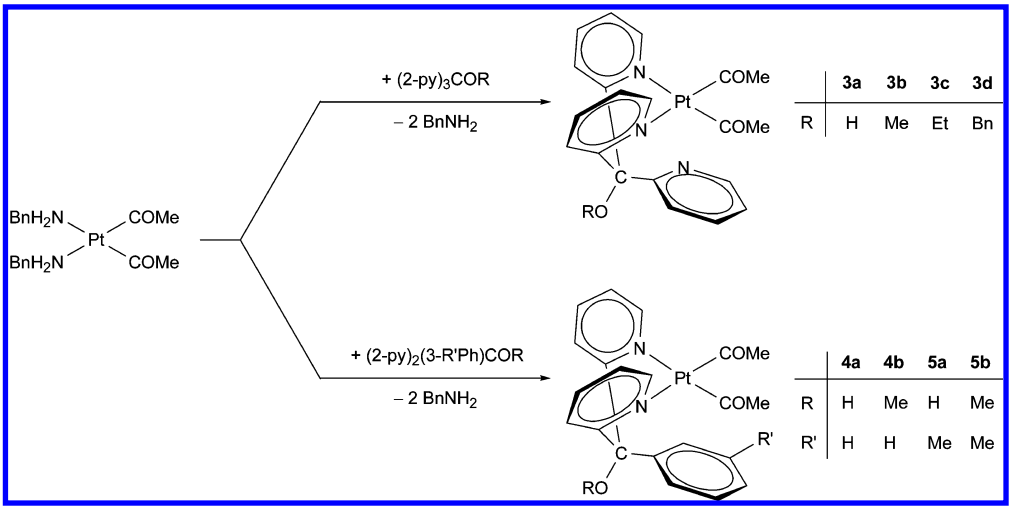

Another class of facially coordinating tripodal ligands, which has received considerable attention in both coordination and organometallic chemistry in recent years, are the neutral tris(2-pyridyl)methanol ligands ($(2\text{-py})_3\text{COH}$) and the respective tris(2-pyridyl)methyl ether ligands ($(2\text{-py})_3\text{COR}$).[9] The main difference from the aforementioned ligand classes is the change of the donating group from pyrazole to pyridine, which is reported to be both a better σ donor and π acceptor ligand than pyrazole.[9,10] Here, we report on the synthesis and characterization of diacetylplatinum(II) complexes bearing κ^2N,N'-coordinated tris(2-pyridyl)methanol and tris(2-pyridyl)methyl ether ligands as well as on the molecular dynamics of these complexes. Furthermore, for comparison, ligands are included which bear a phenyl or *m*-tolyl group instead of the pendant third pyridine ring.

dx.doi.org/10.1021/om400091h | *Organometallics* XXXX, XXX, XXX–XXX

2. RESULTS AND DISCUSSION

2.1. Synthesis of Diacetylplatinum(II) Complexes. Reactions of $[Pt(COMe)_2(NH_2Bn)_2]$ (**2**) with $(2\text{-py})_3COR$ afforded in facile ligand exchange reactions the diacetylplatinum(II) complexes $[Pt(COMe)_2\{(2\text{-py})_3COR\}]$ (R = H (**3a**), Me (**3b**), Et (**3c**), Bn (**3d**)) bearing κ^2 bonded tris(2-pyridyl)methanol (**3a**) and tris(2-pyridyl)methyl ether (**3b**–**d**) ligands (Scheme 2). By the same pathway the structurally similar complexes $[Pt(COMe)_2\{(2\text{-py})_2PhCOR\}]$ (R = H (**4a**), Me (**4b**)) and $[Pt(COMe)_2\{(2\text{-py})_2(m\text{-Tol})COR\}]$ (R = H (**5a**), Me (**5b**)) were prepared, where the pendant pyridyl group of type **3** complexes is replaced by a phenyl (**4**) and a *m*-tolyl group (**5**), respectively (Scheme 2). Thus, in type **4** and **5** complexes the pendant group is symmetrically and unsymmetrically replaced, respectively. All compounds were isolated in good yields between 68 and 90% as yellow solids, which were characterized by NMR (^1H, ^{13}C, ^{195}Pt) and IR spectroscopy as well as by high-resolution mass spectrometric (HRMS-ESI) investigations and single-crystal X-ray diffraction analyses (**3**). All complexes are soluble in methanol, methylene chloride, and chloroform. At room temperature under anaerobic conditions, solutions of compounds **3** are stable for several days, while for solutions of complexes **4** and **5** the start of decomposition can be detected by NMR spectroscopy within 2 days.

As an alternative route to prepare diacetylplatinum(II) complexes, in general, reactions of the respective bi- or tridentate ligands with the platina-β-diketone **1** followed by the reduction of the formed diacetyl(hydrido)platinum(IV) complexes induced by proton abstraction by a base can be envisioned. This is shown in Scheme 1 for the analogous diacetylplatinum(II) complexes bearing scorpionate (**III**) or tris(pyrazolyl)methane ligands (**IV**). Here, in this pathway, only complexes bearing etherified ligands (R = Me, Et, Bn; **3b**–**d**, **4b**, **5b**) could be synthesized. Reactions with the alcohol derivatives (R = H) failed. Due to, in general, poorer yields and a more time-consuming workup procedure, this pathway was not further pursued.

2.2. Structures of $[Pt(COMe)_2\{(2\text{-py})_3COR\}]$ (R = H (3a), Me (3b), Et (3c), Bn (3d)). Crystals of $[Pt(COMe)_2\{(2\text{-py})_3COR\}]$ (R = H (**3a**), Me (**3b**), Et (**3c**), Bn (**3d**)) suitable for X-ray diffraction analyses were obtained from a saturated methylene chloride solution at −7 °C (**3a**·CH_2Cl_2) and from THF solutions layered with *n*-pentane (**3b**–**d**). The molecular structures are shown in Figures 1–4, respectively. Selected structural parameters are given in the figure captions. The platinum atoms are coordinated in a square-planar fashion by two acetyl ligands and the κ^2N,N'-coordinated $(2\text{-py})_3COR$ ligand. The angles between neighboring ligands are all close to 90° (84.3(1)–95.9(1)°, **3a**; 84.4(2)–93.2(2)°, **3b**; 84.2(2)–93.7(2)°, **3c**; 84.2(2)–94.0(2)°, **3d**). The $C(\mu\text{-py})_2Pt$ units adopt a boat conformation with the backbone carbon atom of the $(2\text{-py})_3COR$ ligand (C10) and the platinum atom at the apexes. The noncoordinated pyridine ring is situated in an axial position of this boat structure and oriented pseudo-parallel to the coordination plane (Pt,C1,C3,N2,N4). The angles between the complex plane and the plane of the noncoordinated pyridine ring are between 46.2(2) and 50.7(2)°, resulting in distances of 3.769 Å (**3a**), 3.656 Å (**3b**), 3.681 Å (**3c**), and 3.770 Å (**3d**) between the platinum atom and the center of gravity of the noncoordinated ring. In crystals of complexes **3b**–**d**, the torsion angles C21–O3–C10–C16 (44.3(7)°, **3b**; 47.8(7)°, **3c**; 41.2(7)°, **3d**) demonstrated that the noncoordinated pyridine rings and the substituents R at the oxygen atoms O3 are *gauche* to each other.

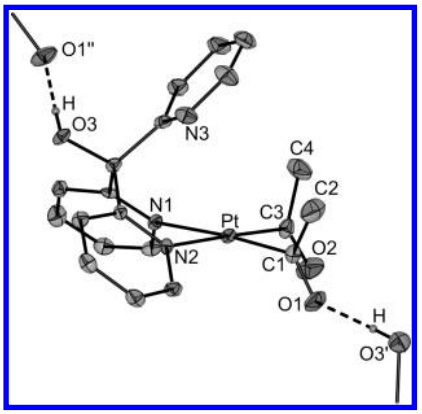

Figure 1. Structure of $[Pt(COMe)_2\{(2\text{-py})_3COH\}]$ (**3a**) in crystals of **3a**·CH_2Cl_2. Ellipsoids are shown at the 30% probability level. H atoms are omitted for clarity, except for that at O3. The broken line indicates an intermolecular O–H···O hydrogen bond in crystals of **3a**·CH_2Cl_2. Selected structural parameters (distances in Å, angles in deg): Pt–C1 = 1.975(4), Pt–C3 = 1.997(4), Pt–N1 = 2.140(3), Pt–N2 = 2.139(3), C1–Pt–C3 = 87.1(2), C1–Pt–N2 = 92.7(1), C3–Pt–N1 = 95.9(1), N1–Pt–N2 = 84.3(1), C1–Pt–N1 = 175.4(1), C3–Pt–N2 = 178.4(2), O1···O3′ = 2.652(4).

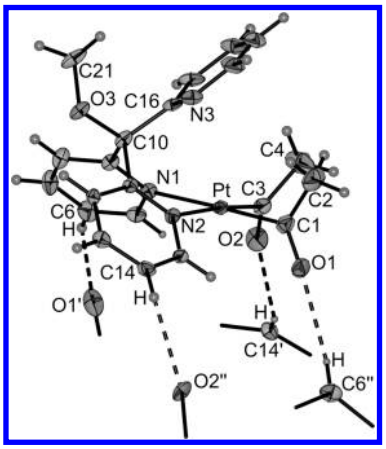

Figure 2. Molecular structure of $[Pt(COMe)_2\{(2\text{-py})_3COMe\}]$ (**3b**). Ellipsoids are shown at the 30% probability level. Broken lines indicate intermolecular C–H···O hydrogen bonds in crystals of **3b**. Selected structural parameters (distances in Å, angles in deg): Pt–C1 = 2.016(7), Pt–C3 = 2.014(6), Pt–N1 = 2.140(5), Pt–N2 = 2.147(4), C1–Pt–C3 = 91.2(3), C1–Pt–N2 = 91.1(2), C3–Pt–N1 = 93.2(2), N1–Pt–N2 = 84.4(2), C1–Pt–N1 = 175.5(2), C3–Pt–N2 = 174.0(4), C21–O3–C10–C16 = 44.3(7), C6···O1′ = 3.35(1), H···O1′ = 2.49, C6–H···O1′ = 151, C14′···O2 = 3.277(8), H···O2 = 2.51, C14′–H···O2 = 139.

In all structures, the carbonyl oxygen atoms of the two acetyl ligands were found to lie on the same side of the complex plane. Thus, the diacetyl moieties represent a "*cisoid*" conformation as a result of intermolecular hydrogen bonds: in crystals of the complex **3a**·CH_2Cl_2 the O1···O3′ distance of 2.652(4) Å indicates the presence of an intermolecular O–H···O hydrogen bond[11] between the acetyl ligand and the hydroxyl group at the backbone C atom of the $(2\text{-py})_3COH$ ligand (Figure 1), such that the crystals are threaded by one-dimensional strands. In crystals of **3b**,**c** the oxygen atoms of the acetyl ligands were found to act as H acceptors in weak

dx.doi.org/10.1021/om400091h | *Organometallics* XXXX, XXX, XXX–XXX

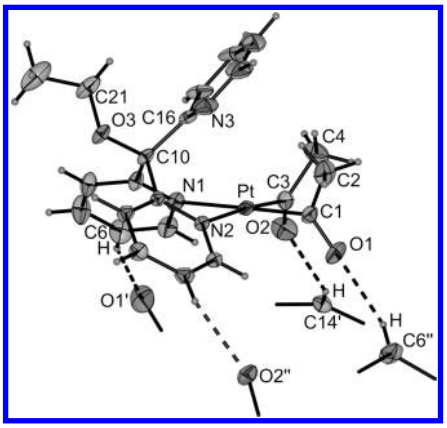

Figure 3. Molecular structure of $[Pt(COMe)_2\{(2\text{-}py)_3COEt\}]$ (**3c**). Ellipsoids are shown at the 30% probability level. Broken lines indicate intermolecular C−H···O hydrogen bonds in crystals of **3c**. Selected structural parameters (distances in Å, angles in deg): Pt−C1 = 1.998(6), Pt−C3 = 2.009(6), Pt−N1 = 2.143(4), Pt−N2 = 2.157(4), C1−Pt−C3 = 89.8(2), C1−Pt−N2 = 92.3(2), C3−Pt−N1 = 93.7(2), N1−Pt−N2 = 84.2(2), C1−Pt−N1 = 176.5(2), C3−Pt−N2 = 174.3(4), C21−O3−C10−C16 = 47.8(7), C6···O1′ = 3.25(1), H···O1′ = 2.37, C6−H···O1′ = 155, C14′···O2 = 3.189(9), H···O2 = 2.43, C14′−H···O2 = 137.

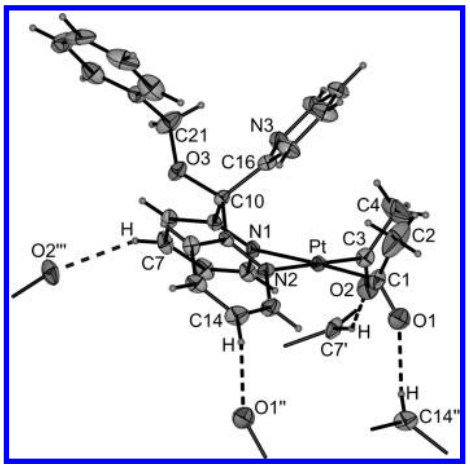

Figure 4. Molecular structure of $[Pt(COMe)_2\{(2\text{-}py)_3COBn\}]$ (**3d**). Ellipsoids are shown at the 30% probability level. Broken lines indicate intermolecular C−H···O hydrogen bonds in crystals of **3d**. Selected structural parameters (distances in Å, angles in deg): Pt−C1 = 2.007(6), Pt−C3 = 2.010(6), Pt−N1 = 2.142(4), Pt−N2 = 2.156(4), C1−Pt−C3 = 88.6(2), C1−Pt−N2 = 93.2(2), C3−Pt−N1 = 94.0(2), N1−Pt−N2 = 84.2(2), C1−Pt−N1 = 176.9(2), C3−Pt−N2 = 177.9(2), C21−O3−C10−C16 = 41.2(7), C7′···O2 = 3.272(8), H···O2 = 2.44, C7′−H···O2 = 147, C14″···O1 = 3.313(8), H···O1 = 2.38, C14″−H···O1 = 170.

intermolecular C_{py}−H···O hydrogen bonds, so that the crystals are built up by strands in a zigzag manner, as shown in Figure 5 for complex **3b** as an example. The structural parameters of all these hydrogen bonds (C···O = 3.189(9)−3.35(1) Å, O···H = 2.37−2.51 Å, C−H···O = 137−170°) are in the range expected for such attractive interactions.[12] In contrast, in crystals of **3d** the C_{py}−H···O hydrogen bonds built up a three-dimensional network.

2.3. Spectroscopic Investigations. The ^1H, ^{13}C, and ^{195}Pt NMR spectra of the diacetylplatinum(II) complexes **3**−**5** give proof of their identities. At room temperature, in the ^1H and ^{13}C NMR spectra of **3b**−**d** and **5b** some signals are broadened, pointing to a dynamic process. Thus, low-temperature and temperature-dependent NMR measurements in CD_3OD were also performed.

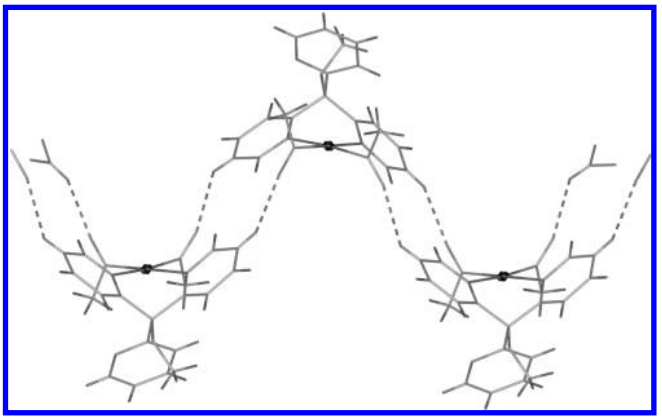

Figure 5. Wire model showing the zigzag arrangement of the molecules in crystals of **3b**.

At room temperature, the ^1H NMR spectrum of $[Pt(COMe)_2\{(2\text{-}py)_3COH\}]$ (**3a**) displayed one signal for both acetyl ligands and two sets of signals with a 2:1 intensity in the aromatic area reflecting a mirror-symmetric structure of the complex in solution. In contrast, at room temperature, the ^1H NMR spectra of $[Pt(COMe)_2\{(2\text{-}py)_3COR\}]$ (R = Me (**3b**), Et (**3c**), Bn (**3d**)) exhibited broad signals for the protons both of the acetyl ligands and of the coordinated pyridine rings, as shown in Figure 6 for complex **3b**. At −20 °C, these signals were found to be split up, indicating a dynamic process that leads to a loss of the mirror-symmetric structure of the complexes in solution (Table 1). In contrast, the ^1H NMR spectrum of **3a** (R = H) recorded even at −80 °C still displayed only one sharp signal for the acetyl ligands and—in addition to the signals of the pendant pyridyl group—only one set of signals for the protons of the two coordinated pyridine rings.

The similar type **4** and **5** complexes $[Pt(COMe)_2\{(2\text{-}py)_2PhCOR\}]$ (R = H (**4a**), Me (**4b**)) and $[Pt(COMe)_2\{(2\text{-}py)_2(m\text{-}Tol)COH\}]$ (**5a**), where the pendant pyridyl group is replaced by a phenyl or *m*-tolyl group, do not show any dynamics, whereas the complex $[Pt(COMe)_2\{(2\text{-}py)_2(m\text{-}Tol)\text{-}COMe\}]$ (**5b**) shows a dynamics (although not all proton signals are split up) analogous to that of complexes **3b**−**d** (Table 1). Thus, in compliance with complexes **3**, the dynamics depend on both the symmetry of the pendant group (unsymmetrically substituted as py, *m*-Tol versus symmetrically substituted as Ph) and the substitution pattern at the backbone C atom (OR with R = Me, Et, Bn versus OH).

In general, the same observations were made in the ^{13}C NMR spectra of compounds **3**−**5**. At room temperature, spectra of **3b**−**d** and **5b** exhibited broad signals (which split up at lower temperatures) or even two sets of signals for the C atoms of the acetyl ligands and of the coordinated pyridine rings. On the other hand, the ^{13}C NMR room-temperature spectra of **3a**, **4**, and **5a** reflect a mirror-symmetric structure of the complexes in solution.

The conditions for the existence of mirror-symmetric structures in solution should be both a fast rotation of the acetyl ligands and a fast rotation of the substituent R at the backbone of the $(2\text{-}py)_3COR$ ligand as well as of the noncoordinated pyridine/*m*-tolyl ring. Since a hindered rotation of the acetyl ligands can be excluded due to experience with a number of other diacetylplatinum(II) complexes,[5,7,13]

dx.doi.org/10.1021/om400091h | *Organometallics* XXXX, XXX, XXX−XXX

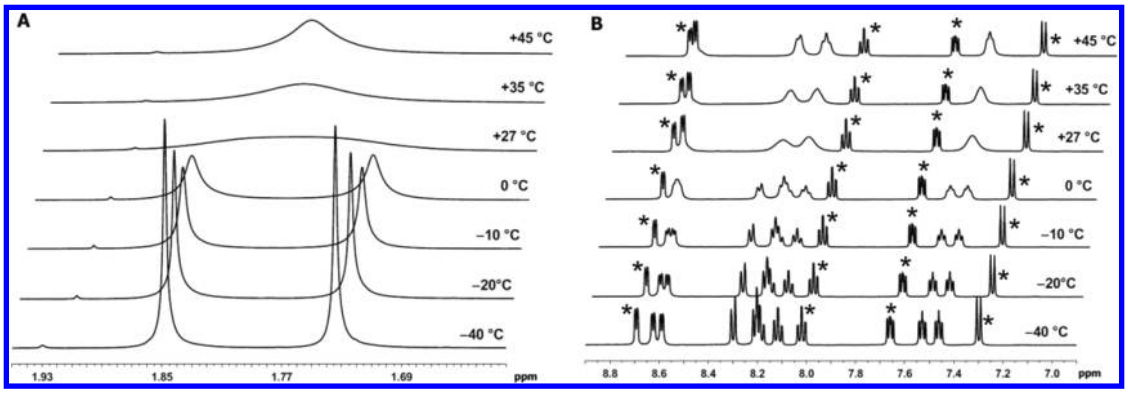

Figure 6. Variable-temperature ^{1}H NMR spectra of **3b** measured in CD_3OD: (A) region related to the acetyl ligands.; (B) aromatic region. Signals of the noncoordinated pyridyl group are marked with asterisks.

Table 1. Temperature-Dependent Characteristic Proton Shifts (in ppm) of the Acetyl Ligands and of the Coordinated Pyridyl Groups of $[Pt(COMe)_2\{(2\text{-py})_3COR\}]$ (R = Me (3b), Et (3c), Bn (3d)) and $[Pt(COMe)_2\{(2\text{-py})_2(m\text{-Tol})COMe\}]$ (5b)[a]

	T (°C)	δ_{acetyl}	δ_{H3}	δ_{H4}	δ_{H5}	δ_{H6}
3b[b]	+27	1.79	8.21	8.11	7.44	8.62
	−20	1.74/1.85	8.20/8.29	8.11/8.18	7.45/7.52	8.60/8.63
3c[b]	+27	1.79	8.21	8.11	7.44	8.62
	−20	1.73/1.85	8.19/8.28	8.11/8.19	7.45/7.52	8.60/8.63
3d[b]	+27	1.80	8.26	8.12	7.45	8.65
	−20	1.75/1.85	8.21/8.33	8.10/8.18	7.45/7.52	8.62/8.64
5b[b]	+27	1.76	8.20	8.10	ca. 7.4[e]	8.65
	−20	1.72/1.80	8.22	8.13	ca. 7.4[e]	8.61/8.67
3a[b]	+27	1.76	8.38	8.10	7.43	8.59
4a[c]	+27	1.71	8.43	7.96	7.25	8.64
4b[d]	+27	1.79	8.04	7.88	7.25	8.83
5a[b]	+27	1.74	8.40	8.10	7.43	8.63

[a]For comparison, the corresponding values of complexes **3a**, **4a,b**, and **5a** without dynamics are shown. [b]Measured in $CDOD_3$. [c]Measured in CD_2Cl_2. [d]Measured in $CDCl_3$. [e]Overlapped with other signals.

these results imply that in complexes **3b−d** and **5b** at least one of the other aforementioned rotations is hindered and thus is the reason for the observed phenomena in NMR spectroscopy.

To get an impression of the thermodynamic parameters of these potentially hindered rotations, the signals of the acetyl ligands were used for an analysis of this dynamics by NMR techniques. Thus, variable-temperature ^{1}H NMR studies were performed to estimate the coalescence temperatures. Furthermore, from line-shape analyses[14] of spectra recorded in a range close to the coalescence temperatures (283−318 K), the activation parameters $\Delta H^{\ddagger}$ and $\Delta S^{\ddagger}$ have been determined by Eyring plots (Figure 7). The Gibbs free energies of activation at the coalescence temperature were calculated according to $\Delta G_C^{\ddagger} = \Delta H^{\ddagger} - T_C \cdot \Delta S^{\ddagger}$. The compilation of $\Delta G_C^{\ddagger}$ and related parameters in Table 2 shows that the coalescence temperatures (296−303 K) as well as the Gibbs free energies of activation at the coalescence temperature (14.6−15.8 kcal mol^{-1}) for all compounds were found in a narrow range. The enthalpies of activation (ca. 9.2 kcal mol^{-1}) and entropies of activation (ca. −18.7 cal mol^{-1} K^{-1}) calculated for complexes **3b−d** are in a narrow range as well. In contrast, the corresponding values of complex **5b** were found to be $\Delta H^{\ddagger}$ = 12.8 kcal mol^{-1} and $\Delta S^{\ddagger}$ = −8.5 cal mol^{-1} K^{-1}, thus being higher by about 2.6 kcal mol^{-1} and about 10.2 cal mol^{-1} K^{-1}, respectively. For comparison, the requisite values of the well-studied dimethylformamide as the "benchmark" are given: $\Delta G_C^{\ddagger}$ = 21.5 kcal mol^{-1} at T_C = 114 °C;[15] ΔH = 21.2 kcal mol^{-1}, ΔS = −1.6 cal mol^{-1} K^{-1}.[16]

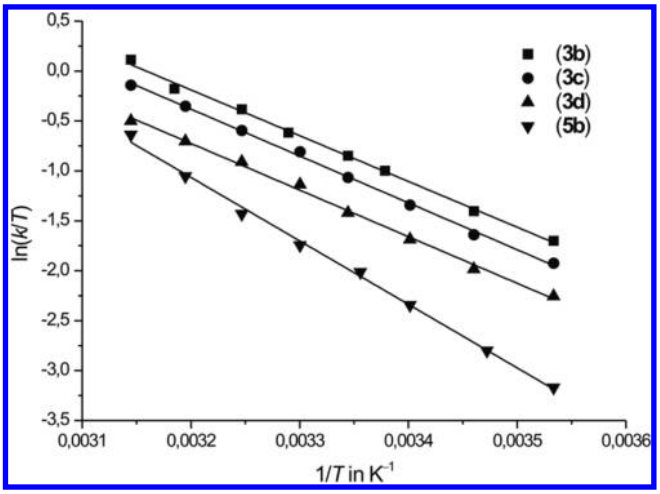

Figure 7. Eyring plots of complexes $[Pt(COMe)_2\{(2\text{-py})_3COR\}]$ (R = Me (**3b**), Et (**3c**), Bn (**3d**)) and $[Pt(COMe)_2\{(2\text{-py})_2(m\text{-Tol})COMe\}]$ (**5b**).

2.4. DFT Calculations. For an additional qualitative and quantitative analysis of the dynamics found in complexes **3b−d** and **5b**, quantum-chemical calculations on the DFT level of theory were performed using the B3LYP functional and high-quality basis sets for all atoms and a pseudopotential for Pt considering relativistic effects (for details, see the Experimental Section). In all calculations solvent effects (MeOH) were

dx.doi.org/10.1021/om400091h | *Organometallics* XXXX, XXX, XXX−XXX

Table 2. Gibbs Free Energies of Activation and Related Parameters for the Dynamics in Complexes 3b–d and 5b

	$\Delta H^{\ddagger}$ (kcal mol^{-1})	$\Delta S^{\ddagger}$ (cal mol^{-1} K^{-1})	$\Delta G_C^{\ddagger}$ (kcal mol^{-1})	T_C (K)
3b	9.1 ± 0.5	−18.5 ± 1.4	14.6 ± 0.8	296
3c	9.3 ± 0.3	−18.2 ± 1.0	14.8 ± 0.6	301
3d	9.2 ± 0.4	−19.1 ± 1.4	15.0 ± 0.8	303
5b	12.8 ± 0.9	−8.5 ± 3.0	15.4 ± 1.8	302

considered according to Tomasi's polarized continuum model.[17] To analyze the dynamics, the complexes [Pt(COMe)$_2${(2-py)$_3$COMe}] (**3b**) and [Pt(COMe)$_2${(2-py)$_2$(*m*-Tol)COMe}] (**5b**) were chosen. Furthermore, for comparison, the complex [Pt(COMe)$_2${(2-py)$_3$COH}] (**3a**) showing a mirror-symmetric structure even at −80 °C was included into the calculations.

At first the equilibrium structures of reasonable conformers (four for each complex) were calculated: see Figure 8 for **3b***[27] and the Supporting Information for **3a*** and **5b***. The standard Gibbs energies ($\Delta G^{\ddagger}$) are given in Table 3. As expected, in all structures the C(μ-py)$_2$Pt units adopt a boat conformation with the platinum atom and the backbone carbon atom of the (2-py)$_3$COR or the (2-py)$_2$(*m*-Tol)COMe ligand at the apexes. In the global minimum (Table 3, entry 1), the OR groups are equatorially positioned, while the asymmetric pendant groups (py in **3a***/**3b***, *m*-Tol in **5b***) are in an axial position and are thus curled toward the platinum center. Moreover, the substituents R and the pendant rings (py/*m*-Tol) are in mutually *gauche* positions. These conformations (R = H (**3a***(py$_{ax}$/*gauche*)); R = Me (**3b***(py$_{ax}$/*gauche*), **5b***(Tol$_{ax}$/*gauche*))) were found in crystals of type **3** complexes except for the *transoid* position of the acetyl ligands which is—in general—favored over a *cisoid* position.[6] The *cisoid* position found in crystals of **3** is a consequence of intermolecular hydrogen bonds (see section 2.2).

The conformers having an *anti* (fully staggered) conformation of the R−O−C−C$_i$ dihedral angle (instead of a *gauche* conformation) are 4.2−5.7 kcal mol^{-1} higher in their standard Gibbs free energies (Table 3, entry 2), which might be caused by steric interactions. Furthermore, two conformers, each with an inverted boat unit, have to be considered. This results in an equatorial position of the pendant pyridyl/*m*-tolyl groups (py$_{eq}$/Tol$_{eq}$). Moreover, the N−C$_i$−C−O dihedral angles (for **5b*** C$_2$−C$_i$−C−O) can be *syn* or *anti*. All these conformers are, at least, 3.2 kcal mol^{-1} higher in their standard Gibbs energies (Table 3, entries 3 and 4).

Table 3. Calculated Standard Gibbs Free Energies (in kcal mol^{-1}) of the Conformers of 3a*, 3b*, and 5b* Relative to the Most Stable Conformer

entry	conformer	**3a***	**3b***	**5b***
1	py$_{ax}$/*gauche*[a]	0	0	0
2	py$_{ax}$/*anti*[a]	4.2	5.5	5.7
3	py$_{eq}$/*syn*[b]	7.2	9.5	6.9
4	py$_{eq}$/*anti*[b]	3.2	5.3	6.4

[a]Conformation characterized by the R−O−C−C$_i$ dihedral angle (C$_i$ = *ipso*-C atom of the pyridine and tolyl ring, respectively). [b]Conformation determined by the N−C$_i$−C−O (for **5b*** C$_2$−C$_i$−C−O) dihedral angle.

As discussed in section 2.3, the dynamics observed may be caused by a hindered rotation of the asymmetric pendant group and/or of the substituent R. In Figure 9 the Gibbs free energy diagram for the rotation of the pendant pyridyl group is shown starting from the most stable *gauche* conformers of **3a*** and **3b***. Here and in the following, the dynamics of **5b*** are very similar to those of **3b***; thus, the diagrams for **5b*** are only given in the Supporting Information. Apart from these conformers (py$_{ax}$/*gauche*; Figure 9, **a**) only one further equilibrium structure each could be located. They are also py$_{ax}$/*gauche* conformers (Figure 9, **c**), their energies being only slightly above the global minima. In the case of **3a*** (R = H), the two activation barriers (Figure 9, **b**/**d**) are significantly different; thus, a flip-flop-type motion could be operative: the activation barrier of the flip-flop-type motion where the N atom of the pendant pyridine ring is directed toward the substituent R = H (Figure 9, **a** → **c** via **b**) is 4.2 kcal mol^{-1}, whereas that where the 3-C−H group of the pendant pyridine ring is directed toward the substituent R = H (Figure 9, **a** → **c** via **d**) is 13.7 kcal mol^{-1}. In the case of **3b*** (R = Me) the two activation barriers (Figure 9, **b**/**d**) are of the same order of magnitude (17.8/19.5 kcal mol^{-1}) and are significantly higher than that for **3a***. Thus, for **3b***, even at room temperature, a rotation of the pendant pyridine group is expected to be hindered.

In Figure 10 the Gibbs free energy diagram for the rotation of R for the complexes **3a*** and **3b*** is shown. An inspection of the Newman projections makes it clear that a rotation of the substituent R by 360° includes the following conversions: *gauche* (Figure 10, **a**; global minimum; R pointed toward the N atom of the pyridine ring) → *anti* (Figure 10, **c**) → *gauche* (Figure 10, **e**; lone electron pair of the O atom pointed toward the N atom) → *gauche* (Figure 10, **a**; global minimum). Obviously, the activation barriers (Figure 10, **b**/**d**) are mainly a

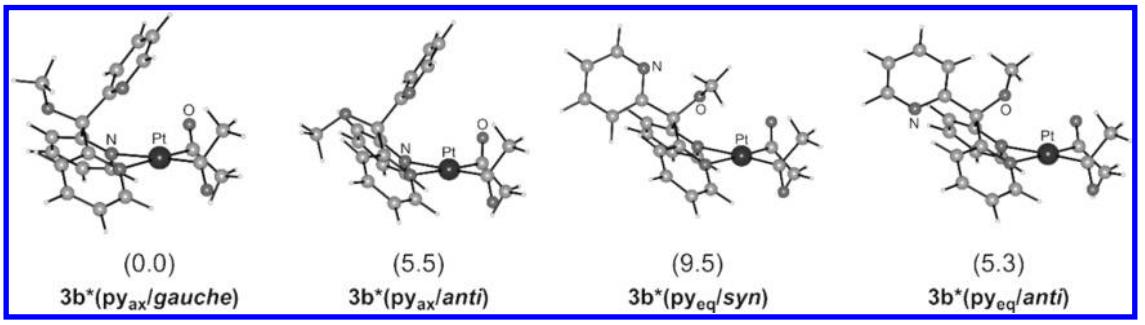

Figure 8. Calculated equilibrium structures of different conformers of [Pt(COMe)$_2${(2-py)$_3$COMe}] (**3b***). The conformers are designated with indices showing an axial (py$_{ax}$) or equatorial (py$_{eq}$) position of the noncoordinated pyridine group and characterizing the dihedral angles R−O−C−C$_i$ (*gauche*, *anti*) and N−C$_i$−C−O (*syn*, *anti*) (C$_i$ = *ipso*-C atom of the noncoordinated pyridine ring), respectively. The standard Gibbs free energies (in kcal mol^{-1}) are given in parentheses relative to the most stable conformer.

dx.doi.org/10.1021/om400091h | *Organometallics* XXXX, XXX, XXX−XXX

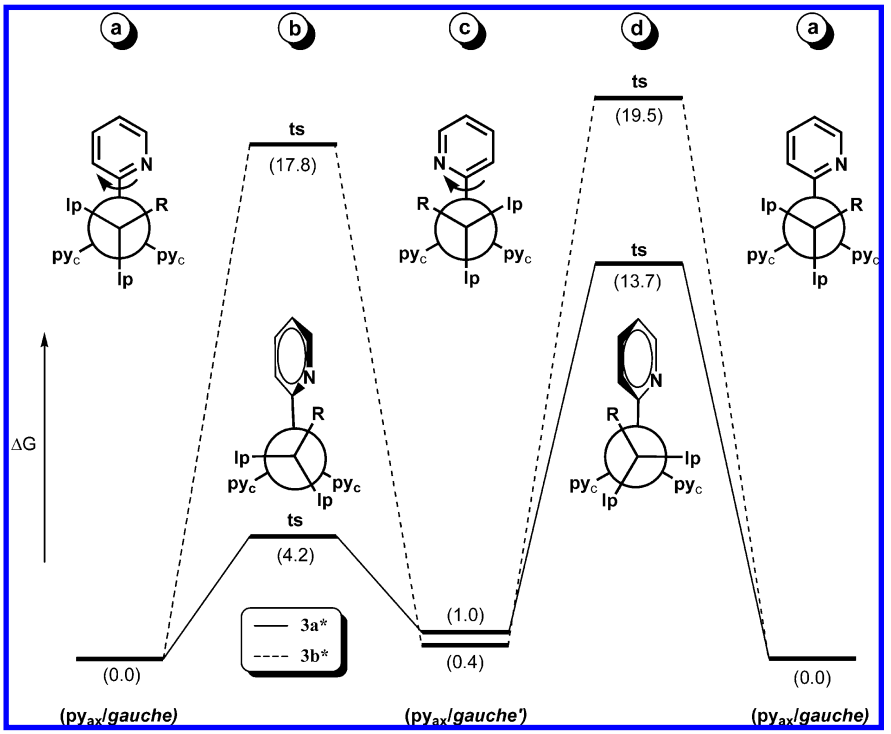

Figure 9. Gibbs free energy diagram for the rotation of the noncoordinated pyridyl group in $[Pt(COMe)_2\{(2\text{-}py)_3COR\}]$ (R = H (**3a***) Me (**3b***)). The Gibbs energies (in kcal mol^{-1}) are given in parentheses relative to the most stable isomer (**ts** = transition state). The Newman projections (lp = lone electron pair; py_c = coordinated pyridyl) are along the O−C vector of the backbone of the $(2\text{-}py)_3COR$ (R = H, Me) ligands.

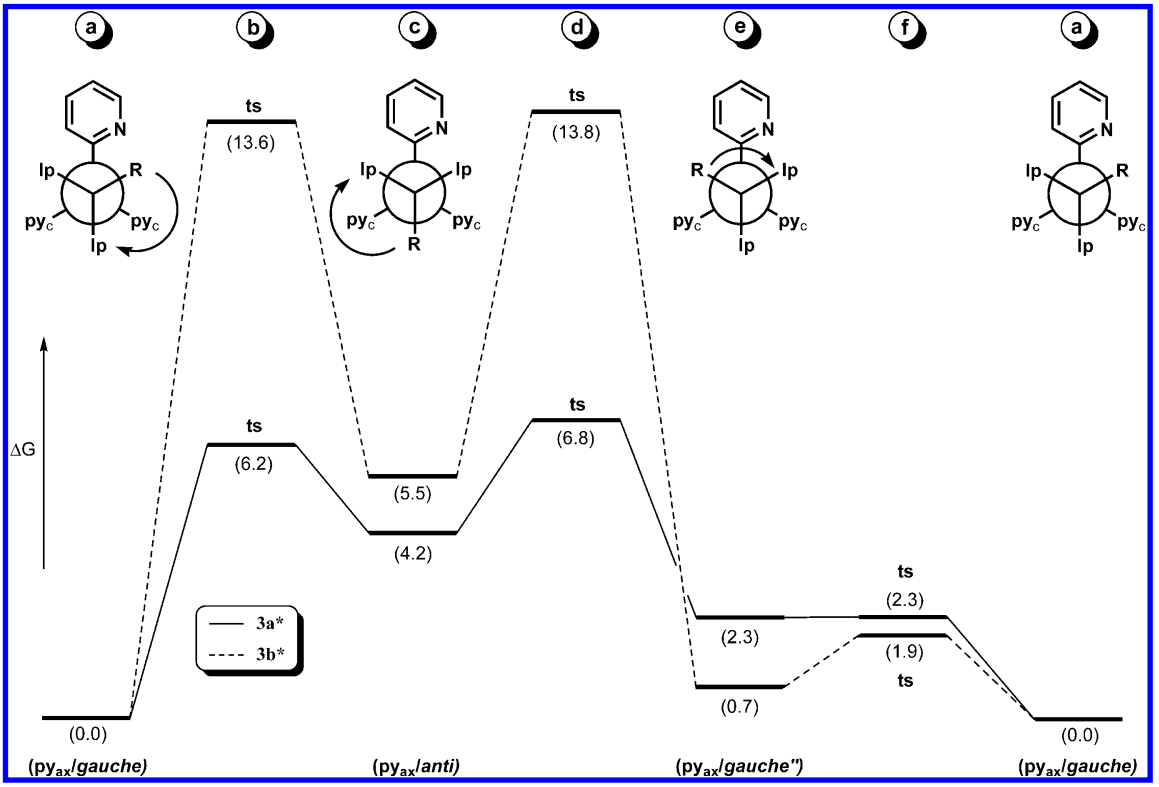

Figure 10. Gibbs free energy diagram for the rotation of the substituent R in $[Pt(COMe)_2\{(2\text{-}py)_3COR\}]$ (R = H (**3a***), Me (**3b***)). The Gibbs energies (in kcal mol^{-1}) are given in parentheses relative to the most stable isomer (**ts** = transition state). The Newman projections (lp = lone electron pair; py_c = coordinated pyridyl) are along the O−C vector of the backbone of the $(2\text{-}py)_3COR$ (R = H, Me) ligands.

consequence of steric repulsion between the substituent R and the 3-CH groups of the coordinated pyridine rings (py_c). Thus, as expected, for R = H (**3a***) the barriers are remarkably lower than for R = Me (**3b***): 6.2/6.8 vs 13.6/13.8 kcal mol^{-1}.

dx.doi.org/10.1021/om400091h | *Organometallics* XXXX, XXX, XXX−XXX

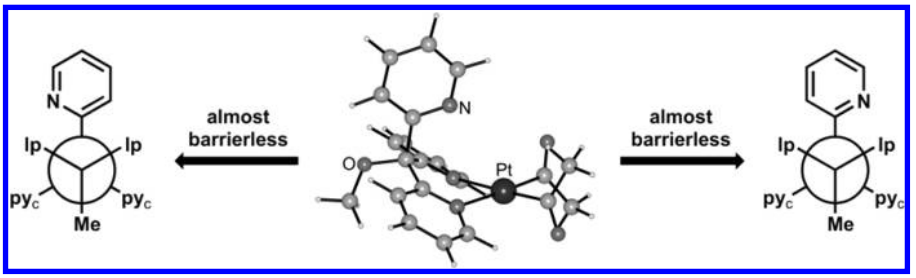

Figure 11. Calculated equilibrium structure of the *anti* conformer **3b***(py$_{ax}$/*anti*) with the N atom of the pendant pyridine ring aligned toward the Pt atom.

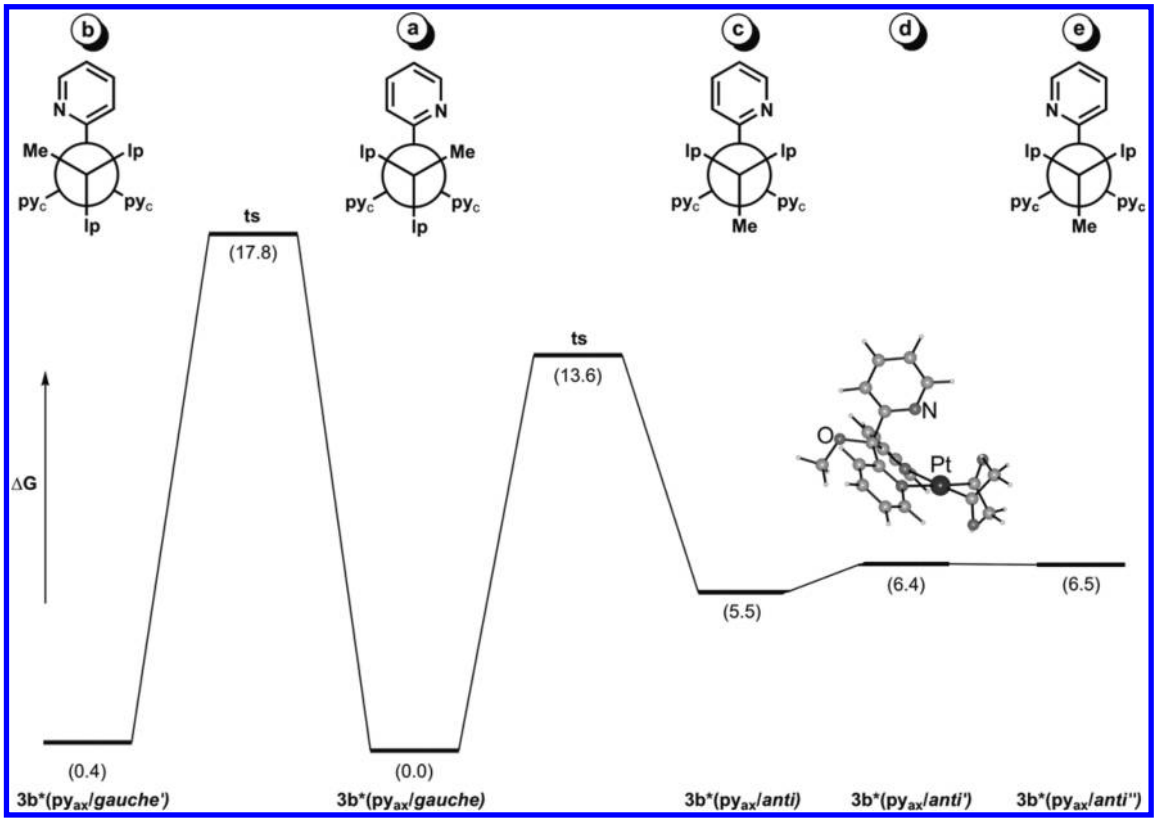

Figure 12. Gibbs free energy diagram for the dynamics in [Pt(COMe)$_2${(2-py)$_3$COMe}] (**3b***). The Gibbs energies (in kcal mol^{-1}) are given in parentheses relative to the most stable isomer (**ts** = transition state). The Newman projections (lp = lone electron pair; py$_c$ = coordinated pyridyl) are along the O−C vector of the backbone of the (2-py)$_3$COMe ligand.

Since for the *gauche* conformer of **3b*** the activation barriers for the rotation of the pendant pyridine ring (Figure 9, **b**/**d**) are significantly higher than those calculated for the *gauche*−*anti* isomerization (17.8/19.5 vs 13.6/13.8 kcal mol^{-1}), calculations concerning the rotation of the pendant groups of the *anti* conformers were performed. In addition to the equilibrium structure of the thermodynamically most stable *anti* conformer described above (**3b***(py$_{ax}$/*anti*) in Figure 8), another one (**3b***(py$_{ax}$/*anti''*)) was found lying 0.9 kcal mol^{-1} over the aforementioned one (Figure 11). In this structure the pendant pyridyl group is positioned perpendicular to the complex plane while the N atom is aligned toward the Pt atom. The rotation of 90° both clockwise and anticlockwise was found to be almost barrierless; thus, a flip-flop-type motion could be operative (Figure 11). In contrast, a similar structure having the C−H group oriented toward the Pt atom is a transition state, which lies in its Gibbs free energy 3.6 kcal mol^{-1} above the most stable *anti* conformer (see the Gibbs free energy diagram in Figure S2 (Supporting Information)).

For the rotation of the *m*-tolyl group in the *anti* conformer of **5b*** only insignificant activation barriers were found, and thus, a 360° rotation could be operative in this case. Although irrelevant (because the *gauche*−*anti* isomerization is higher in Gibbs free energy than the flip-flop-type motion of the pyridyl group in the *gauche* conformer), the rotation of the pyridine ring in the *anti* conformer of **3a*** was calculated. In this case two activation barriers of 6.2 and 7.3 kcal mol^{-1} were found (see the Gibbs free energy diagram in Figure S1 (Supporting Information)).

All structures of the conformers with the inverted boat structure (py$_{eq}$/*syn* and py$_{eq}$/*anti*) lie between 3.2 and 6.9 kcal mol^{-1} above the global minimum equilibrium structures (py$_{ax}$/*gauche*). Furthermore, for the inversion of the boat structure (which might proceed according a dissociative mechanism),[18] a relatively high barrier can be assumed. Thus, although it cannot

dx.doi.org/10.1021/om400091h | *Organometallics* XXXX, XXX, XXX−XXX

be strictly ruled out, these conformers should not play a role in the dynamics observed.

2.5. Conclusions. Within this work, the synthesis and characterization of diacetylplatinum(II) complexes bearing κ^2-bonded ligands of type $(2\text{-py})_3$COR (R = H, Me, Et, Bn), $(2\text{-py})_2$PhCOR, and $(2\text{-py})_2$(*m*-Tol)COR (R = H, Me) have been described. Furthermore, both a qualitative and quantitative analyses of the dynamics found in complexes **3b**−**d** and **5b** bearing asymmetric pendant groups (py/*m*-Tol) and etherified ligands (R ≠ H) by NMR techniques and DFT calculations have been presented. The results of the DFT calculations indicate that the dynamics observed is caused by an interplay of a hindered and unhindered rotation, respectively, of the substituent R and/or of the pendant py/*m*-Tol group.

(1) For complexes with an etherified ligand (R ≠ H) and an asymmetric pendant pyridyl group (**3b**−**3d**; in the following discussed with **3b*** as an example) it can be stated that, starting from the *gauche* conformer, the activation barrier for the *gauche*−*anti* isomerization (Figure 12, **a** → **c**) is remarkably lower than that for the rotation of the pendant pyridyl group (Figure 12, **a** → **b**). For the *anti* conformer a flip-flop-type motion of the pendant group (py) has an insignificant activation barrier and thus is favorable (Figure 12, **c** → **e** via **d**). In accordance with the NMR experiments, the mirror symmetry of complexes in solution is retained, at least at higher temperatures, due to the activation barrier of 13.6 kcal mol^{-1} (**3b***) for the *gauche*−*anti* isomerization.

(2) The situation of complex **5b** having an etherified ligand (R = Me) and an asymmetric pendant *m*-tolyl group is analogous to that described above, but—instead of a flip-flop-type motion of the pendant group in the *anti* conformer—a full 360° rotation takes place, which proved to be nearly barrierless (see Figure S5 (Supporting Information) for **5b***).

(3) For complexes with an alcohol group (R = H) and an asymmetric pendant pyridyl or *m*-tolyl group (**3a**, **5a**; in the following discussed with **3a*** as an example, see Figures 12 and 10) it can be stated that a flip-flop-type motion of the pendant group of the *gauche* conformer (global minimum) retains the mirror symmetry, whereas the *gauche*−*anti* isomerization does not play a role. In accordance with the NMR experiments, due to the activation barrier of 4.2 kcal mol^{-1}, the dynamics are operative even at lower temperatures.

(4) For complexes with a symmetric pendant phenyl group (**4a**,**b**), irrespective whether the ligand is etherified (R = Me) or not (R = H), mirror-symmetric structures were observed NMR spectroscopically. Obviously, the situation is analogous to the *m*-tolyl complex **5b***, but due to the symmetric pendant phenyl group a loss of the complex symmetry due to hindered rotation is irrelevant.

The present study gives a detailed insight into the nature of the dynamics in diacetylplatinum(II) complexes bearing κ^2N,N'-coordinated ligands of types $(2\text{-py})_3$COR, $(2\text{-py})_2$PhCOR, and $(2\text{-py})_2$(*m*-Tol)COR. Moreover, a very good agreement between the values obtained from NMR experiments (ΔG_{298} = 14.6 kcal mol^{-1} (**3b**), 14.7 kcal mol^{-1} (**3c**), 14.9 kcal mol^{-1} (**3d**), 15.3 kcal mol^{-1} (**5b**)) and from DFT calculations (ΔG_{298} = 13.6/14.5 kcal mol^{-1} (**3b***/**5b***)) was found.

Thus, overall there are three types of diacetylplatinum(II) complexes with κ^2N,N'-coordinated ligands having an additional pendant *N*-donor site at their disposal, namely type **III** complexes (see Scheme 1) with anionic tris(pyrazolyl)borate ligands, type **IV** complexes (see Scheme 1) with neutral tris(pyrazolyl)methane ligands, and complexes of type **3** with neutral tris(pyridyl)methanol and tris(pyridyl)methyl ether ligands discussed here. In type **IV** complexes, molecular rearrangement (exchange of coordinated and noncoordinated pyrazolyl rings via intermediates having only κ^1N-coordinated ligands) was observed, pointing to a weak coordination of the neutral tris(pyrazolyl)methane ligands.[6] Type **III** complexes do not show any molecular dynamics, indicating, as expected, a stronger coordination of the scorpionate ligands due to their negative charge.[5] In the neutral type **3** complexes discussed here, which have pyridine type donor sites, the molecular dynamics observed are due to a rotation or a flip-flop-type motion of the pendant (noncoordinated) pyridine group but not due to a decoordination/recoordination mechanism as in type **IV** complexes. This is in accord with a stronger σ donor ability of pyridine in comparison with that of pyrazole.[9] Thus, the donor ability of such ligands depends both on the overall charges of the ligands and complexes, respectively, and on the nature of the donor N atoms.

3. EXPERIMENTAL SECTION

3.1. General Comments. All reactions were performed under an argon atmosphere using standard Schlenk techniques. Solvents were dried (diethyl ether and THF over Na/benzophenone) and distilled prior to use. If not otherwise stated, NMR spectra were recorded at 27 °C with Varian VXR 400 and Unity 500 spectrometers. Chemical shifts are relative to solvent signals ($CDCl_3$, δ_H 7.24, δ_C 77.0; CD_2Cl_2, δ_H 5.32, δ_C 53.8; CD_3OD δ_H 3.31, δ_C 49.0) as internal references; $\delta(^{195}Pt)$ is referenced to $Na_2[PtCl_6]$. If necessary, 2D NMR techniques (H,H C,H COSY, HMBC, and NOESY) were used to assign the signals in ^1H and ^{13}C NMR spectra. Temperature calibration for variable-temperature measurements was performed using CD_3OD.[19] IR spectra were recorded with a Bruker Tensor 28 spectrometer with a Platinum ATR unit. Microanalyses were performed by the University of Halle microanalytical laboratory using a CHNS-932 (LECO) elemental analyzer. The high-resolution ESI mass spectra were obtained from a Bruker Apex III Fourier transform ion cyclotron resonance (FT-ICR) mass spectrometer (Bruker Daltonics) equipped with an Infinity cell, a 7.0 T superconducting magnet (Bruker), an rf-only hexapole ion guide, and an external APOLLO electrospray ion source (Agilent, off-axis spray). The sample solutions were introduced continuously via a syringe pump with a flow rate of 120 μL h^{-1}. The complexes $[Pt_2\{(COMe)_2H\}_2(\mu\text{-}Cl)_2]$ (**1**) and $[Pt(COMe)_2(NH_2Bn)_2]$ (**2**) were prepared according to literature methods.[1,7] Syntheses and spectroscopic data of the ligands, which, in part, have not yet been described in the literature, are reported in the Supporting Information.

3.2. Syntheses of the Diacetylplatinum(II) Complexes (3−5). $[Pt(COMe)_2(NH_2Bn)_2]$ (**2**; 100 mg, 0.2 mmol) and an equimolar amount of the respective ligand were dissolved in THF (5 mL) and stirred for 30 min. The volume of the yellow solution was reduced in vacuo to about 2 mL, and diethyl ether (8 mL) was added. The yellow precipitate that formed was filtered off, washed with diethyl ether (3 × 2 mL), and dried in vacuo.

*3.2.1. [Pt(COMe)$_2${(2-py)$_3$COH}] (**3a**).* Yield: 87 mg (80%). HRMS (ESI): *m*/*z* calcd for $[C_{20}H_{19}O_3N_3PtH]^+$ 545.11487, found for $[M - H]^+$ 545.11456. ^1H NMR (400 MHz, CD_3OD): δ 1.76 (s, 6H, $COCH_3$), 7.10 (m, 1H, H^9 py), 7.43 (m, 2H, $H^{5/5'}$ py), 7.49 (m, 1H, H^{11} py), 7.89 (m, 1H, H^{10} py), 8.10 (m, 2H, $H^{4/4'}$ py), 8.38 (m, 2H, $H^{3/3'}$ py), 8.56 (m, 1H, H^{12} py), 8.59 (m, 2H, $H^{6/6'}$ py). ^{13}C NMR (100 MHz, CD_3OD): δ 43.9 (s + d, $^3J_{Pt,H}$ = 343.7 Hz, $COCH_3$), 85.0 (s, $(2\text{-py})_3COH$), 124.6 (s, C^{11} py), 125.0 (s, $C^{3/3'}$ py), 125.5 (s, $C^{5/5'}$ + C^9 py), 138.8 (s, C^{10} py), 140.7 (s, $C^{4/4'}$ py), 150.5 (s, C^{12} py), 152.2 (s, $C^{6/6'}$ py), 162.5 (s, $C^{2/2'}$ py), 164.8 (s, C^8 py), 236.5 (s + d, $^3J_{Pt,H}$ = 1286.9 Hz, $COCH_3$). Here and in the following, the two coordinated pyridine rings are numbered 1−6 and 1′−6′, respectively; noncoordinated pyridine rings are numbered 7−12. ^{195}Pt NMR (107

dx.doi.org/10.1021/om400091h | *Organometallics* XXXX, XXX, XXX−XXX

MHz, CD_2Cl_2): δ −3221.8 (s). IR: ν(CO) 1624, ν(CO) 1601, ν(CO) 1576, ν(CO) 1562 cm^{-1}.

*3.2.2. [Pt(COMe)$_2${(2-py)$_3$COMe}] (**3b**).* Yield: 82 mg (73%). HRMS (ESI): m/z calcd for $[C_{21}H_{21}O_3N_3PtH]^+$ 559.13053, found for $[M - H]^+$ 559.13046. ^{1}H NMR (500 MHz, CD_3OD, −20 °C): δ 1.74 (s, 3H, $COCH_3$), 1.85 (s, 3H, $COCH_3$), 3.29 (s, 3H, OCH_3), 7.28 (m, 1H, H^9 py), 7.45/7.52 (m, 2H, H^5 + $H^{5'}$ py), 7.64 (m, 1H, H^{11} py), 8.00 (m, 1H, H^{10} py), 8.11/8.18 (m, 2H, H^4 + $H^{4'}$py), 8.20/8.29 (m, 2H, H^3 + $H^{3'}$py), 8.60/8.63 (m, 2H, H^6 + $H^{6'}$ py), 8.69 (m, 1H, H^{12} py). ^{1}H NMR (500 MHz, CD_3OD, +27 °C): δ 1.79 (s (br), 6H, $COCH_3$), 3.29 (s, 3H, OCH_3), 7.22 (m, 1H, H^9 py), 7.44 (s (br), 2H, $H^{5/5'}$ py), 7.59 (m, 1H, H^{11} py), 7.96 (m, 1H, H^{10} py), 8.11 (s (br), 2H, $H^{4/4'}$ py), 8.21 (s (br), 2H, $H^{3/3'}$ py), 8.62 (m, 2H, $H^{6/6'}$ py), 8.66 (m, 1H, H^{12} py). ^{13}C NMR (50 MHz, CD_2Cl_2, −80 °C): δ 43.4/43.5 (s, 2 × $COCH_3$), 53.6 (s, OCH_3), 88.2 (s, (2-py)$_3$COMe), 122.6/123.1/123.2/123.6/124.2/125.7 (s, C^3 + $C^{3'}$ + C^9 + C^5 + $C^{5'}$ + C^{11} py), 136.2 (s, C^{10} py), 138.3/138.7 (s, C^4 + $C^{4'}$ py), 149.2/150.4/151.3 (s, C^6 + $C^{6'}$ + C^{12}py), 156.9/158.2/159.6 (s, C^2 + $C^{2'}$ + C^8 py), 229.0/230.3 (s, 2 × $COCH_3$). ^{13}C NMR (100 MHz, CD_2Cl_2, +27 °C): δ 43.5 (s (br), $COCH_3$), 54.1 (s, OCH_3), 89.4 (s, (2-py)$_3$COMe), 123.5 (s (br), $C^{3/3'}$ py), 123.8 (s, C^{11} py), 124.1/124.6 (s (br), C^5 + $C^{5'}$ py), 126.5 (s, C^9 py), 136.8 (s, C^{10} py), 138.8 (s (br), $C^{4/4'}$ py), 149.8 (s, C^{12} py), 151.5/152.6 (s (br), C^6 + $C^{6'}$ py), 158.9/161.1 (s (br), C^2 + $C^{2'}$ py), 159.3 (s, C^8 py), 226.6/227.8 (s (br), 2 × $COCH_3$). ^{195}Pt NMR (107 MHz, CD_2Cl_2): δ −3221.8 (s). IR: ν(CO) 1600, ν(CO) 1583, ν(CO) 1564 cm^{-1}.

*3.2.3. [Pt(COMe)$_2${(2-py)$_3$COEt}] (**3c**).* Yield: 97 mg (85%). HRMS (ESI): m/z calcd for $[C_{22}H_{23}O_3N_3PtH]^+$ 545.14619, found for $[M - H]^+$ 573.14627. ^{1}H NMR (500 MHz, CD_3OD, −20 °C): δ 1.40 (t, 3H, OCH_2CH_3), 1.73 (s, 3H, $COCH_3$), 1.85 (s, 3H, $COCH_3$), 3.30 (m, 2H, OCH_2CH_3), 7.25 (m, 1H, H^9 py), 7.45/7.52 (s, 2H, H^5 + $H^{5'}$), 7.63 (m, 1H, H^{11} py), 7.99 (m, 1H, H^{10} py), 8.11/8.19 (s, 2H, H^4 + $H^{4'}$ py), 8.19/8.28 (s, 2H, H^3 + $H^{3'}$ py), 8.60/8.63 (m, 2H, H^6 + $H^{6'}$ py), 8.67 (m, 1H, H^{12} py). ^{1}H NMR (500 MHz, CD_3OD, +27 °C): δ 1.33 (t, 3H, OCH_2CH_3), 1.79 (s (br), 6H, $COCH_3$), 3.33 (s, (br), 2H, OCH_2CH_3), 7.19 (m, 1H, H^9 py), 7.44 (s (br), 2H, $H^{5/5'}$ py), 7.57 (m, 1H, H^{11} py), 7.94 (m, 1H, H^{10} py), 8.11 (s (br), 2H, $H^{4/4'}$ py), 8.21 (s (br), 2H, $H^{3/3'}$ py), 8.62 (m, 2H, $H^{6/6'}$ py), 8.64 (m, 1H, H^{12} py). ^{13}C NMR (100 MHz, CD_3OD, −20 °C): δ 15.5 (s, OCH_2CH_3), 43.9/44.2 (s, 2 × $COCH_3$), 63.0 (s, OCH_2CH_3), 89.9 (s, (2-py)$_3$COEt), 125.0/125.1/125.3/125.6/126.2/127.9 (s, C^3 + $C^{3'}$ + C^9 + C^5 + $C^{5'}$ + C^{11} py), 138.9/140.9/141.3 (s, C^4 + $C^{4'}$ + C^{10} py), 150.5/152.0/153.1 (s, C^6 + $C^{6'}$ + C^{12} py), 159.8/160.8/161.7 (s, C^2 + $C^{2'}$ + C^8 py), 235.4/237.7 (s, 2 × $COCH_3$).^{13}C NMR (100 MHz, CD_2Cl_2, +27 °C): δ 15.4 (s, OCH_2CH_3), 43.5 (s (br), $COCH_3$), 62.0 (s, OCH_2CH_3), 89.2 (s, (2-py)$_3$COEt), 123.4 (s (br), $C^{3/3'}$ py), 123.6 (s, C^{11} py), 124.1/124.7 (s (br), C^5 + $C^{5'}$ py), 126.3 (s, C^9 py), 136.8 (s, C^{10} py), 138.8/139.9 (s (br), C^4 + $C^{4'}$ py), 149.7 (s, C^{12} py), 151.4/152.5 (s (br), C^6 + $C^{6'}$ py), 159.2/161.3 (s (br), C^2 + $C^{2'}$ py), 159.9 (s, C^8 py), 227.2/228.4 (s (br), 2 × $COCH_3$). ^{195}Pt NMR (107 MHz, CD_2Cl_2): δ −3213.4 (s). IR: ν(CO) 1615, ν(CO) 1585 cm^{-1}.

*3.2.4. [Pt(COMe)$_2${(2-py)$_3$COBn}] (**3d**).* Yield: 89 mg (70%). HRMS (ESI): m/z calcd for $[C_{27}H_{25}O_3N_3PtH]^+$ 635.16188, found for $[M - H]^+$ 635.16155. ^{1}H NMR (500 MHz, CD_3OD, −20 °C): δ 1.75 (s, 3H, $COCH_3$), 1.85 (s, 3H, $COCH_3$), 4.42 (m, 2H, OCH_2Ph), 7.30 (m, 1H, H^9 py), 7.33 (m, 1H, *p*-C*H* Ph), 7.39 (m, 2H, *m*-C*H* Ph), 7.44 (m, 2H, *o*-C*H* Ph), 7.45/7.52 (s, 2H, H^5 + $H^{5'}$ py), 7.61 (m, 1H, H^{11} py), 7.96 (m, 1H, H^{10} py), 8.10/8.18 (s, 2H, H^4 +$H^{4'}$ py), 8.21/8.33 (s, 2H, H^3 + $H^{3'}$ py), 8.62/8.64 (m, 2H, H^6 + $H^{6'}$ py), 8.68 (m, 1H, H^{12} py). ^{1}H NMR (500 MHz, CD_3OD, +27 °C): δ 1.80 (s (br), 6H, $COCH_3$), 4.44 (s (br), 2H, OCH_2Ph), 7.23 (m, 1H, H^9 py), 7.30 (m, 1H, *p*-C*H* Ph), 7.35−7.42 (m, 4H, *o*-C*H* + *m*-C*H* Ph), 7.45 (s (br), 2H, $H^{5/5'}$ py), 7.56 (m, 1H, H^{11} py), 7.90 (m, 1H, H^{10} py), 8.12 (s (br), 2H, $H^{4/4'}$ py), 8.26 (s (br), 2H, $H^{3/3'}$ py), 8.65 (m, 3H, $H^{6/6'}$ + H^{12} py). ^{13}C NMR (50 MHz, $CDCl_3$, −80 °C): δ 43.5/43.6 (s, 2 × $COCH_3$), 67.0 (s, OCH_2Ph), 88.2 (s, (2-py)$_3$COBn), 122.7/123.1/123.4/123.7/124.3/125.3 (s, C^3 + $C^{3'}$ + $C^{9'}$ + $C^{5'}$ + C^5 + C^{11} py), 126.4/128.1 (s, *m*- + *o*-CH Ph), 127.4 (s, *p*-C*H* Ph), 136.6 (s, C^{10} py), 136.7 (s, *i*-C Ph), 138.5/138.7 (s, $C^{4'}$ + C^4 py), 149.2/150.6/151.3 (s, C^6 + $C^{6'}$ + C^{12} py), 157.2/158.5/159.1 (s, C^2 + $C^{2'}$ + C^8 py), 229.2/230.2 (s, 2 × $COCH_3$). ^{13}C NMR (125 MHz, $CDCl_3$, +27 °C): δ 43.3/43.6 (s (br), 2 × $COCH_3$), 67.9 (s, OCH_2Ph), 89.1 (s, (2-py)$_3$COBn), 122.8/123.0 (s (br), $C^{3/3'}$ py), 123.5 (s, C^{11} py), 123.7/124.5 (s (br), C^5 + $C^{5'}$ py), 126.6 (s, C^9 py), 127.1 (s, *m*-C*H* Ph), 128.0 (s, *o*-C*H* Ph), 128.6 (s, *p*-C*H* Ph), 136.6 (s, C^{10} py), 137.2 (s, *i*-C Ph), 138.6 (s (br), $C^{4/4'}$ py), 149.5 (s, C^{12} py), 151.5/153.1 (s (br), C^6 + $C^{6'}$ py), 158.4/160.8 (s (br), C^2 + $C^{2'}$ py), 158.8 (s, C^8 py), 226.4/229.5 (s (br), 2 × $COCH_3$). ^{195}Pt NMR (107 MHz, CD_2Cl_2): δ −3213.4 (s). IR: ν(CO) 1614, ν(CO) 1583 cm^{-1}.

*3.2.5. [Pt(COMe)$_2${(2-py)$_2$PhCOH}] (**4a**).* Yield: 98 mg (90%). HRMS (ESI): m/z calcd for $[C_{21}H_{20}O_3N_2PtH]^+$ 544.11965, found for $[M - H]^+$ 544.11945. ^{1}H NMR (500 MHz, CD_2Cl_2): δ 1.71 (s, 6H, $COCH_3$), 6.92 (m, 2H, *o*-C*H* Ph), 7.25 (m, 2H, $H^{5/5'}$ py), 7.32 (m, 2H, *m*-C*H* Ph), 7.39 (m, 1H, *p*-C*H* Ph), 7.96 (m, 2H, $H^{4/4'}$ py), 8.43 (m, 2H, $H^{3/3'}$ py), 8.64 (m, 2H, $H^{6/6'}$ py). ^{13}C NMR (125 MHz, +27 °C, CD_2Cl_2): δ 43.2 (s + d, $^2J_{Pt,C}$ = 355.2 Hz, $COCH_3$), 82.9 (s, (2-py)$_2$PhCOH), 123.7 (s, $C^{3/3'}$ py), 124.0 (s, $C^{5/5'}$ py), 128.3 (s, *p*-C*H* Ph), 128.4 (s, *o*-C*H* Ph), 128.8 (s, *m*-C*H* Ph), 138.7 (s, $C^{4/4'}$ py), 145.8 (s, *i*-C Ph), 151.4 (s, $C^{6/6'}$ py), 161.2 (s, $C^{2/2'}$ py), 230.5 (s + d, $^1J_{Pt,C}$ = 1304.7 Hz, $COCH_3$). ^{195}Pt-NMR (107 MHz, CD_2Cl_2): δ −3249.4 (s). IR: ν(CO) 1599, ν(CO) 1576 cm^{-1}.

*3.2.6. [Pt(COMe)$_2${(2-py)$_2$PhCOMe}] (**4b**).* Yield: 87 mg (78%). HRMS (ESI): m/z calcd for $[C_{22}H_{22}O_3N_2PtH]^+$ 558.13531, found for $[M - H]^+$ 558.13487. ^{1}H NMR (400 MHz, $CDCl_3$): δ 1.79 (s, 6H, $COCH_3$), 3.18 (s, 3H, OCH_3), 6.95 (m, 2H, *o*-C*H* Ph), 7.25 (m, 2H, $H^{5/5'}$ py), 7.39−7.44 (m, 3H, *m*-C*H* + *p*-C*H* Ph), 7.88 (m, 2H, $H^{4/4'}$ py), 8.04 (m, 2H, $H^{3/3'}$ py), 8.83 (m, 2H, $H^{6/6'}$ py). ^{13}C NMR (125 MHz, +27 °C, $CDCl_3$): δ 43.5 (s + d, $^2J_{Pt,C}$ = 377.6 Hz, $COCH_3$), 88.4 (s, (2-py)$_2$PhCOH), 122.8 (s, $C^{3/3'}$ py), 123.9 (s, $C^{5/5'}$ py), 128.6 (s, *m*-C*H* Ph), 128.8 (s, *p*-C*H* Ph), 130.4 (s, *m*-C*H* Ph), 138.3 (s, $C^{4/4'}$ py), 139.2 (s, *i*-C Ph), 152.5 (s, $C^{6/6'}$ py), 160.0 (s, $C^{2/2'}$ py), 230.5 (s + d, $^1J_{Pt,C}$ = 1304.7 Hz, $COCH_3$). ^{195}Pt NMR (107 MHz, $CDCl_3$): δ −3206.3 (s). IR: ν(CO) 1599, ν(CO) 1576 cm^{-1}.

*3.2.7. [Pt(COMe)$_2${(2-py)$_2$(m-Tol)COH}] (**5a**).* Yield: 80 mg (72%). HRMS (ESI): m/z calcd for $[C_{22}H_{22}O_3N_2PtH]^+$ 558.13531, found for $[M - H]^+$ 558.13508. ^{1}H NMR (400 MHz, CD_3OD): δ 1.74 (s, 6H, $COCH_3$), 2.30 (s, 3H, 3-CH_3Ph), 6.72 (m, 1H, H^6 *m*-Tol), 6.76 (s, 1H, H^2 *m*-Tol), 7.27−7.34 (m, 2H, H^4 + H^5 *m*-Tol), 7.43 (m, 2H, $H^{5/5'}$ py), 8.10 (s, 2H, $H^{4/4'}$ py), 8.40 (m, 2H, $H^{3/3'}$ py), 8.63 (s, 2H, $H^{6/6'}$ py). ^{13}C NMR (100 MHz, CD_3OD): δ 21.6 (s, 3-CH_3Ph), 43.9 (s, COMe), 53.5 (s, OCH_3), 82.3 (s, (2-py)$_2$(*m*-Tol)COH), 124.9 (s, $C^{3/3'}$ py), 125.4 (s, $C^{5/5'}$ py), 126.9 (s, C^6 *m*-Tol), 130.0 (s, C^4 + C^5 *m*-Tol), 130.6 (s, C^2 *m*-Tol), 139.6 (s, C^3, *m*-Tol), 140.5 (s, $C^{4/4'}$ py), 147.1 (s, C^1 *m*-Tol), 152.4 (s, $C^{6/6'}$ py), 163.2 (s, $C^{2/2'}$ py), 236.9 (s, $COCH_3$). ^{195}Pt NMR (107 MHz, CD_2Cl_2): δ −3244.8 (s). IR: ν(CO) 1618, ν(CO) 1600, ν(CO) 1574 cm^{-1}.

*3.2.8. [Pt(COMe)$_2${(2-py)$_2$(m-Tol)COMe}] (**5b**).* Yield: 78 mg (68%). HRMS (ESI): m/z calcd for $[C_{23}H_{24}O_3N_2PtH]^+$ 545.15097, found for $[M - H]^+$ 572.15109. ^{1}H NMR (500 MHz, CD_3OD, −20 °C): δ 1.72 (s, 3H, $COCH_3$), 1.80 (s, 3H, $COCH_3$), 2.34 (s, 3H, 3-CH_3Ph), 3.24 (s, 3H, OCH_3), 6.77 (m, 1H, H^6 *m*-Tol), 6.84 (s, 1H, H^2 *m*-Tol), 7.32−7.49 (m, 4H, H^4 + H^5 *m*-Tol + $H^{5/5'}$ py), 8.13 (s, 2H, $H^{4/4'}$ py), 8.22 (m, 2H, $H^{3/3'}$ py), 8.61/8.67 (m, 2H, $H^6/H^{6'}$ py). ^{1}H NMR (500 MHz, CD_3OD, +27 °C): δ 1.76 (s (br), 6H, $COCH_3$), 2.33 (s, 3H, 3-CH_3Ph), 3.25 (s, 3H, OCH_3), 6.76 (m, 1H, H^6 *m*-Tol), 6.81 (s, 1H, H^2 *m*-Tol), 7.31−7.45 (m, 4H, H^4 + H^5 *m*-Tol + $H^{5/5'}$ py), 8.10 (s, 2H, $H^{4/4'}$ py), 8.20 (m, 2H, $H^{3/3'}$ py), 8.65 (s (br), 2H, $H^{6/6'}$ py). ^{13}C NMR (125 MHz, −20 °C, CD_3OD): δ 21.7 (s, 3-CH_3Ph), 43.4/44.1 (s, 2 × COMe), 54.2 (s, OCH_3), 89.6 (s, (2-py)$_2$(*m*-Tol)COH), 125.0/125.2 (s, C^3 + $C^{3'}$ py), 125.7/125.8 (s, C^5 + $C^{5'}$ py), 128.7 (s, C^6 *m*-Tol), 130.0 (s, C^5 *m*-Tol), 130.8 (s, C^4 *m*-Tol), 132.5 (s, C^2 *m*-Tol), 139.6 (s, C^3, *m*-Tol), 140.9/141.0 (s, C^4 + $C^{4'}$ py), 139.1 (s, C^1 *m*-Tol), 152.6/152.9 (s, C^6 + $C^{6'}$ py), 160.9/161.5 (s, C^2 + $C^{2'}$ py), 236.4/237.3 (s, 2 × $COCH_3$). ^{13}C NMR (125 MHz, +27 °C, $CDCl_3$): δ 21.5 (s, 3-CH_3Ph), 43.4 (s (br), COMe), 53.5 (s, OCH_3), 88.4 (s, (2-py)$_2$(*m*-Tol)COH), 122.8 (s (br), $C^{3/3'}$ py), 123.8 (s (br), $C^{5/5'}$ py), 127.4 (s, C^6 *m*-Tol), 128.5, (s, C^5 *m*-Tol), 129.5 (s, C^4 *m*-Tol), 131.1 (s, C^2 *m*-Tol), 138.2 (s, C^3 *m*-Tol), 138.3 (s (br), $C^{4/4'}$ py), 139.1 (s, C^1 *m*-Tol), 152.4 (s (br), $C^{6/6'}$ py), 159.9/160.2 (s (br), C^2 + $C^{2'}$ py),

dx.doi.org/10.1021/om400091h | *Organometallics* XXXX, XXX, XXX−XXX

Table 4. Crystal Data and Structure Refinement for 3a−d

	3a·CH_2Cl_2	3b	3c	3d
empirical formula	$C_{21}H_{21}Cl_2N_3O_3Pt$	$C_{21}H_{21}N_3O_3Pt$	$C_{22}H_{23}N_3O_3Pt$	$C_{27}H_{25}N_3O_3Pt$
formula wt	629.4	558.5	572.5	634.6
cryst syst	monoclinic	orthorhombic	orthorhombic	monoclinic
space group	$P2_1/c$	$P2_12_12_1$	$P2_12_12_1$	$P2_1/c$
a (Å)	8.3991(9)	8.1635(3)	8.2151(7)	14.315(3)
b (Å)	15.800(1)	13.7797(6)	13.932(1)	10.722(1)
c (Å)	17.095(2)	17.8650(7)	18.546(2)	16.602(2)
β (deg)	100.74(1)			108.82(2)
V (Å^3)	2228.4(4)	2009.6(1)	2122.5(3)	2412.1(6)
Z	4	4	4	4
D_{calcd} (g cm^{-3})	1.876	1.846	1.792	1.747
μ(Mo Kα) (mm^{-1})	6.563	7.008	6.638	5.851
F(000)	1216	1080	1112	1240
θ range (deg)	2.43−26.01	2.28−28.00	2.64−25.93	2.30−25.84
no. of rflns collected	15455	11935	12293	16605
nol of obsd rflns ($I > 2\sigma(I)$)	3603	4395	3848	3736
no. of indep rflns	4306 (R_{int} = 0.0741)	4757 (R_{int} = 0.0424)	4080 (R_{int} = 0.0333)	4640 (R_{int} = 0.0569)
no. of data/restraints/params	4306/0/274	4757/0/256	4080/0/264	4640/0/309
goodness of fit on F^2	0.978	1.037	1.047	1.010
final R indices ($I > 2\sigma(I)$)	R1 = 0.0312	R1 = 0.0293	R1 = 0.0250	R1 = 0.0317
	wR2 = 0.0551	wR2 = 0.0546	wR2 = 0.0562	wR2 = 0.0729
R indices (all data)	R1 = 0.0393	R1 = 0.0349	R1 = 0.0280	R1 = 0.0439
	wR2 = 0.0572	wR2 = 0.0558	wR2 = 0.0570	wR2 = 0.0768
largest difference peak, hole (e Å^{-3})	0.893, −0.782	0.776, −0.917	1.064, −0.430	1.418, −1.260

227.8/227.9 (s (br), 2 × $COCH_3$). ^{195}Pt NMR (107 MHz, CD_2Cl_2): δ −3205.2 (s). IR: ν(CO) 1618, ν(CO) 1600, ν(CO) 1573 cm^{-1}.

3.3. X-ray Crystallography. Data for X-ray diffraction analyses of single crystals were collected on a Stoe-IPDS (**3a,b,d**) or a Stoe-IPDS 2T diffractometer (**3b**) at 200 K using Mo Kα radiation (λ = 0.71073 Å, graphite monochromator). A summary of the crystallographic data, the data collection parameters, and the refinement parameters is given in Table 4. Absorption corrections were applied empirically with the PLATON program package (T_{min}/T_{max}: 0.04/0.15, **3a**·CH_2Cl_2; 0.23/0.47, **3b**; 0.10/0.17, **3c**; 0.45/0.71, **3d**).[20] The structures were solved with direct methods using SHELXS-97[21] and refined using full-matrix least-squares routines against F^2 with SHELXL-97.[22] All non-hydrogen atoms were refined with anisotropic displacement parameters and hydrogen atoms with isotropic parameters. H atoms were placed in calculated positions according to the riding model.

3.4. Computational Details. DFT calculations were performed with the Gaussian09 program package[23] using the functional B3LYP.[24] The 6-311++G(d,p) basis sets as implemented in Gaussian09 were employed for main-group atoms, while the relativistic pseudopotential of the Ahlrichs group and related basis functions of TZVPP quality were employed for the Pt atom.[25] The appropriateness of the functional in combination with the basis sets and effective core potential used for reliable interpretation of structural and energetic aspects of related platinum complexes has been demonstrated.[26] All systems were fully optimized without any symmetry restrictions. The resulting geometries were characterized as equilibrium structures and transition states, respectively, by the analysis of the force constants of normal vibrations. Solvent effects (methanol) were considered according to Tomasi's polarized continuum model.[17] The method was used as implemented in Gaussian 09,[23] which is much more sophisticated than in previous Gaussian versions, especially because solvent effects are considered in each optimization step.

■ ASSOCIATED CONTENT

Supporting Information

Text, tables, figures, and CIF files giving synthesis details and spectroscopic data of the ligands, energies and Cartesian coordinates of all calculated molecules, Gibbs free energy diagrams for **5b*** and **3a***/**3b*** (*anti* conformer), and crystallographic data for **3a**·CH_2Cl_2 and **3b−d**. This material is available free of charge via the Internet at http://pubs.acs.org. Supplementary crystallographic data (**3a**·CH_2Cl_2, CCDC 922887; **3b**, CCDC 922888; **3c**, CCDC 922889; **3d**, CCDC 922890) can also be obtained free of charge via http://www.ccdc.cam.ac.uk/deposit.

■ AUTHOR INFORMATION

Notes

The authors declare no competing financial interest.

■ REFERENCES

(1) Steinborn, D.; Gerisch, M.; Merzweiler, K.; Schenzel, K.; Pelz, K.; Bögel, H.; Magull, J. *Organometallics* **1996**, *15*, 2454.
(2) Steinborn, D. *Dalton Trans.* **2005**, 2664.
(3) (a) Gerisch, M.; Bruhn, C.; Vyater, A.; Davies, J. A.; Steinborn, D. *Organometallics* **1998**, *17*, 3101. (b) Vyater, A.; Wagner, C.; Merzweiler, K.; Steinborn, D. *Organometallics* **2002**, *21*, 4369.
(4) (a) Trofimenko, S. *Scorpionates: The Coordination Chemistry of Polypyrazolylborate Ligands*; Imperial College Press: London, 1999. (b) Pettinari, C. *Scorpinates II: Chelating Borate Ligands*; Imperial College Press: London, 2008.
(5) Bette, M.; Rüffer, T.; Bruhn, C.; Schmidt, J.; Steinborn, D. *Organometallics* **2012**, *31*, 3700.
(6) Bette, M.; Schmidt, J.; Steinborn, D. *Eur. J. Inorg. Chem.* **2013**, DOI: 10.1002/ejic.201201468.
(7) Kluge, T.; Bette, M.; Vetter, C.; Schmidt, J.; Steinborn, D. *J. Organomet. Chem.* **2012**, *715*, 93.
(8) Pettinari, C.; Pettinari, R. *Coord. Chem. Rev.* **2005**, *249*, 525.
(9) Szczepura, L. F.; Witham, L. M.; Takeuchi, K. J. *Coord. Chem. Rev.* **1998**, *174*, 5.
(10) Jameson, D. L.; Blaho, J. K.; Kruger, K. T.; Goldsby, K. A. *Inorg. Chem.* **1989**, *28*, 4312.
(11) Jeffrey, G. A. *An Introduction to Hydrogen Bonding*; Oxford University Press,: Oxford, U.K., 1997.
(12) Steiner, T. *Cryst. Rev.* **1996**, *6*, 1.

(13) Werner, M.; Bruhn, C.; Steinborn, D. *J. Organomet. Chem.* **2008**, *693*, 2369.
(14) Budzelaar, P. H. M.; *gNMR, NMR Simulation Program, Version 5.0.6.0*; ivorysoft, Centennial, CO, 2006.
(15) Kessler, K. *Angew. Chem., Int. Ed. Engl.* **1970**, *9*, 219.
(16) Sandström, J. *Dynamic NMR Spectroscopy*; Academic Press: London, 1982.
(17) (a) Cances, E.; Mennucci, B.; Tomasi, J. *J. Chem. Phys.* **1997**, *107*, 3032. (b) Cossi, M.; Barone, V.; Mennucci, B.; Tomasi, J. *Chem. Phys. Lett.* **1998**, *286*, 253. (c) Mennucci, B.; Tomasi, J. *J. Chem. Phys.* **1997**, *106*, 5151.
(18) Jalón, F. A.; Manzano, B. R.; Otero, A.; Rodríguez-Pérez, M. C. *J. Organomet. Chem.* **1995**, *494*, 179.
(19) Findeisen, M.; Brand, T.; Berger, S. *Magn. Reson. Chem.* **2007**, *45*, 175.
(20) (a) *MULscanABS, PLATON for Windows Taskbar v1.15*; University of Glasgow, Glasgow, Scotland, 2008. (b) Spek, A. L. *J. Appl. Crystallogr.* **2003**, *36*, 7.
(21) Sheldrick, G. M., *SHELXS-97, Program for Crystal Structure Solution*; University of Göttingen, Göttingen, Germany, 1998.
(22) Sheldrick, G. M. *SHELXS-97, Program for the Refinement of Crystal Structures*; University of Göttingen, Göttingen, Germany, 1997.
(23) Frisch, M. J.; Trucks, G. W.; Schlegel, H. B.; Scuseria, G. E.; Robb, M. A.; Cheeseman, J. R.; Scalmani, G.; Barone, V.; Mennucci, B.; Petersson, G. A.; Nakatsuji, H.; Caricato, M.; Li, X.; Hratchian, H. P.; Izmaylov, A. F.; Bloino, J.; Zheng, G.; Sonnenberg, J. L.; Hada, M.; Ehara, M.; Toyota, K.; Fukuda, R.; Hasegawa, J.; Ishida, M.; Nakajima, T.; Honda, Y.; Kitao, O.; Nakai, H.; Vreven, T.; Montgomery, J. A., Jr.; Peralta, J. E.; Ogliaro, F.; Bearpark, M.; Heyd, J. J.; Brothers, E.; Kudin, K. N.; Staroverov, V. N.; Kobayashi, R.; Normand, J.; Raghavachari, K.; Rendell, A.; Burant, J. C.; Iyengar, S. S.; Tomasi, J.; Cossi, M.; Rega, N.; Millam, J. M.; Klene, M.; Knox, J. E.; Cross, J. B.; Bakken, V.; Adamo, C.; Jaramillo, J.; Gomperts, R.; Stratmann, R. E.; Yazyev, O.; Austin, A. J.; Cammi, R.; Pomelli, C.; Ochterski, J. W.; Martin, R. L.; Morokuma, K.; Zakrzewski, V. G.; Voth, G. A.; Salvador, P.; Dannenberg, J. J.; Dapprich, S.; Daniels, A. D.; Farkas, Ö.; Foresman, J. B.; Ortiz, J. V.; Cioslowski, J.; Fox, D. J. *Gaussian 09, Revision B.01*; Gaussian, Inc., Wallingford, CT, 2009.
(24) Becke, A. D. *J. Chem. Phys.* **1993**, *98*, 5648.
(25) (a) Weigend, F.; Häser, M.; Patzelt, H.; Ahlrichs, R. *Chem. Phys. Lett.* **1998**, *294*, 143. (b) Leininger, T.; Nicklass, A.; Küchle, W.; Stoll, H.; Dolg, M.; Bergner, A. *Chem. Phys. Lett.* **1996**, *255*, 274. (c) Andrae, D.; Häussermann, U.; Dolg, M.; Stoll, H.; Preuss, H. *Theor. Chim. Acta.* **1990**, *77*, 123.
(26) (a) Steinborn, D.; Schwieger, S. *Chem. Eur. J.* **2007**, *13*, 9668. (b) Werner, M.; Lis, T.; Bruhn, C.; Lindner, R.; Steinborn, D. *Organometallics* **2006**, *25*, 5946. (c) Vetter, C.; Kaluderović, G. N.; Paschke, R.; Gómez-Ruiz, S.; Steinborn, D. *Polyhedron* **2009**, *28*, 3699. (d) Schwieger, S.; Heinemann, F. W.; Wagner, C.; Kluge, R.; Damm, C.; Israel, G.; Steinborn, D. *Organometallics* **2009**, *28*, 2485.
(27) Throughout the paper calculated complexes are marked with an asterisk. The index in parentheses is explained in the caption of Figure 8.